Publisher: Taylor & Francis

Journal: *Expert Review of Ophthalmology*

DOI: 10.1080/17469899.2017.1307105

A Review of Feature-based Retinal Image Analysis

Authors: Kirsty C Jordan*[1], Matteo Menolotto[1], Nigel M Bolster[1], Iain AT Livingstone[2] and Mario E Giardini[1].

1 University of Strathclyde – Biomedical Engineering, Wolfson Centre 106 Rottenrow Street, Glasgow G4 0NW, UK

2 Ophthalmology, NHS Forth Valley, Falkirk Community Hospital, Westburn Avenue, Falkirk, UK

*Author for correspondence: kirsty.jordan@strath.ac.uk

Abstract

Introduction: Retinal imaging is a fundamental tool in ophthalmic diagnostics. The potential use of retinal imaging within screening programs, with consequent need to analyze large numbers of images with high throughput, is pushing the digital image analysis field to find new solutions for the extraction of specific information from the retinal image. **Areas covered:** The aim of this review is to explore the latest progress in image processing techniques able to recognize specific retinal image features and potential features of disease. In particular, this review aims to describe publically available retinal image databases, highlight different performance evaluators commonly used within the field, outline current approaches in feature-based retinal image analysis and to map related trends. **Expert Commentary:** This review found two key areas to be addressed for the future development of automatic retinal image analysis: fundus image quality and the affect image processing may impose on relevant clinical information within the images. Performance evaluators of the algorithms reviewed are very promising, however absolute values are difficult to interpret when validating system suitability for use within clinical practice.

Keywords: feature extraction, retinal images, segmentation, fundoscopy, image processing, fundus imaging, retinal photography, retina

1. Introduction

In medical practice, the role of image analysis to assist clinical decision making has spread across all specialties, including ophthalmology [1]. The complex task of obtaining clinically relevant information from a fundus image is the result of the ophthalmologist's knowledge, training and experience. One of the most ambitious objectives for computer scientists is to transfer these learning and decision-making mechanisms into algorithms able to assist the physicians in performing this task [2].

The urgency to achieve this goal has been highlighted by the WHO as a result of the recent epidemiological studies regarding diabetic retinopathy (DR), age-related macular degeneration (AMD), glaucoma and other ocular pathologies [3,4]. Retinal imaging technology has proven to be very effective for screening and detection of pathologies of the fundus [5], serving as a powerful diagnostic tool in ophthalmology, boosting the image data acquisition process. Furthermore, the development of community-specific retinal imaging solutions, such as leveraging mobile health technology, overcomes the need for skilled personnel to capture images, allowing retinal images to be acquired within the community, even when trained personnel is not available, such as in middle and low-income countries [6,7]. This scenario is challenging healthcare delivery infrastructure with the problem of analyzing the resulting increasingly large number of images. Advancements in computing technology have provided scientists with solutions, which enable analysis of vast quantities of data in an acceptable timeframe.

The main issue to solve is the translation of digital image information into meaningful content for the clinicians, in terms of clinical relevance. In digital imaging, an image is essentially described as a two-dimensional matrix of image points (pixels), each with their own discrete intensity level and spatial position [8]. The general approach for image feature extraction involves several stages, typically: a pre-processing stage for contrast enhancement or non-uniformity equalization, image segmentation, feature extraction and image classification [9]. In order to mimic the human diagnostic process, an algorithm must therefore apply some rules or constraints to detect a pattern, a trend, or a common characteristic within the pixels [10].

This review aims to offer an overview of recent developments of feature extraction techniques for fundus images. Clinicians extract information from images relying on different image features, such as color, shape, contrast, depending on the features analyzed. Similarly, in image processing, the information extraction strategy varies according to the retinal object involved. To underline this

conceptual path, in this review we have divided the feature extraction techniques according to the retinal object concerned.

2. Retinal image databases

The availability of publicly accessible image databases is a key factor underpinning the development of feature extraction strategies. Procedures such as algorithm validation or training require an increasing amount of data to be processed. This necessity has driven several research groups to make their own retinal image datasets publically available. This trend resulted in the generation of databases with a wide variety of different pathological signs in high resolution. Most databases include the ground truth of pathologies or manual segmentation of the retinal components (optic nerve head (ONH), blood vessel network and macula), and instructions for use. This allows comparison of the performance of algorithms within the same fundus image, with reference to the reliable implementation of a gold-standard procedure. A brief summary of the publicly available databases encountered in the course of this review is given, sorted by clinical target, highlighting their respective advantages for feature-based algorithm development. For convenience, the main characteristics and the key information of each database are summarized in Table 1.

2.1 Optic Nerve Head - *DRIONS–DB (Digital Retinal Images for Optic Nerve Segmentation Database)* – Public database of retinal images for ONH segmentation [11], consisting of 110 color digital retinal images. The optic disc (OD) contour was annotated by two medical experts with 36 landmarks.

RIM-ONE – Fundus image database with accurate gold standards for the ONH evaluation provided by different experts [12]. It includes stereo images from healthy eyes and glaucomatous eyes at different stages. The last release (RIM-ONE Release 3), provides 159 images. Ground truth measurements of the OD and optic cup (OC) are provided by two ophthalmology experts.

2.2 Blood Vessels - *DRIVE (Digital Retinal Images for Vessel Extraction)* – Also known as Utrecht database, was released to enable comparative studies on segmentation of blood vessels [13]. 40 color fundus images randomly selected from a DR screening program in the Netherlands; seven of these contain signs of mild early DR. The dataset is divided into two sets of 20 images, for training and testing of machine learning algorithms [14,15]. For both sets, manual segmentation of the vasculature is available. The DRIVE website allows researchers to share the results of performance of their respective algorithms for vessel segmentation implemented using this database.

REVIEW (Retinal Vessel Image set for Estimation of Widths) – Designed to support the evaluation of techniques for measuring retinal vessel width [16]. 16 images with 193 vessel segments manually identified, divided into 4 sub-sets (described in Table 1), showing a variety of pathologies and vessel types. The image sets contain 5066 manually marked profiles.

CHASE_DB1 (Child Heart Health Study in England) – 28 color images of ocular fundi from 14 multi-ethnic patients in the Child Heart and Health Study in England program [17,18]. Ocular imaging was carried out in over 1000 British primary school children to demonstrate associations between retinal vessel tortuosity and early risk factors for cardiovascular disease. It contains two groups of images characterized by having non-uniform background illumination, poor contrast of blood vessels as compared with the background and wider arterioles with a bright central vessel reflex. The vessel segmentation is provided by two different observers.

HRF (High-Resolution Fundus) Image Database – Created to support comparative studies on automatic segmentation algorithms on ocular fundus images, this public database contains 45 images: 15 healthy patients, 15 DR patients and 15 Glaucoma patients [19]. From the webpage, the manual vessel segmentation and the OD detection are made available for each retinal image.

STARE (STructured Analysis of the Retina) – Part of a project initiated in 1975 by Michael Goldbaum, at the University of California, San Diego (USA), for feature analysis in retinal images [20]. Composed

of 400 images, giving a wide range of anatomical and pathological features alongside manual segmentations. Manual blood vessel segmentation and artery/vein labelling is provided; ONH detection algorithms are also proposed [21]. 44 different pathological features were identified and linked to 13 different pathologies.

VICAVR – Retinal images used for the computation of artery/vein classification [22]. The database currently contains 58 OD-centered images, including the caliber of the vessels measured at different radii from the OD, as well as the vessel type labelled by three experts.

INSPIRE-AVR – Released by a research group at the University of Porto (Portugal) as part of a retinal computer-aided diagnostic system development (RetinaCAD), aimed at the early diagnosis of diabetes, hypertension and cardiovascular pathologies [23-25]. It contains 40 high-resolution OD-centered images complete with ground truth of blood vessels and OD, and the arteriolar-to-venular ratio. The reference standard of the vasculature was obtained by an expert who manually labelled the vessel centerline segments in each image. The OD boundary of each image was approximated by an ellipse fitted to 16 points marked up by an expert. The arteriolar-to-venular ratio values were estimated by an automatic method.

BioImLab – Created by the Laboratory of Biomedical Imaging at the University of Padova (Italy) for retinal vessel tortuosity evaluation [26]. 60 images of retinal vessels from 34 subjects (normal and hypertensive) and information about their manually estimated tortuosity are included.

2.3 Abnormalities **-** *ImageRet* – Collated to develop image processing methods to assist the diagnosis of DR, split into two sub-databases, DIARETDB0 and DIARETDB1 (now implemented in DIARETDB1 V2.1) [27,28]. The first contains 130 color fundus images, 20 normal and 110 with signs of DR. The second consists of 89 color fundus images, 84 containing at least mild non-proliferative signs of DR, 5 are not pathological. Expert annotated ground truth for several well-known diabetic fundus lesions (exudates, microaneurysms and hemorrhages) are also provided.

Messidor – So far, the largest database available of retinal images released to improve the development of automatic diagnostic algorithms for DR [29]. 1200 color fundus photographs with two diagnostic assessments of the retinopathy grade and the risk of macula edema by a medical expert are provided.

e-ophtha – Designed for research in DR, it contains color fundus images obtained from the examinations of patients during 2008-2009 through the OPHDIAT network [30]. Divided into two sub databases, e-ophtha-MA (MicroAneurysms), and e-ophtha-EX (EXudates). e-ophtha-MA contains 148 images with microaneurysms or small hemorrhages and 233 images with no lesion. e-ophtha-EX contains 47 images with exudates and 35 images with no lesion. Both datasets contain a manual segmentation of relevant abnormalities.

The datasets *HEI-MED* and *ARIA*, used in some recent works, are no longer publicly available from the links referenced. Nevertheless, because they were employed in the validation process of some of the techniques taken in consideration, they are briefly described.

HEI-MED (Hamilton Eye Institute Macular Edema Dataset) – The HEI-MED project collects 169 retinal images, with a reasonable mixture of ethnicities and disease state, to train and test algorithm performance of hard exudate detection and diabetic macular edema assessment [31]. Collected from a telemedicine network program for DR diagnosis, it was developed by the Hamilton Eye Institute, the Image Science and Machine Vision Group at ORNL with the collaboration of the University of Bourgogne. The images were graded by an expert into three quality levels, poor, good and excellent.

ARIA - Acquired by clinicians of St. Pauls Eye Unit and University of Liverpool (UK) it consists of 450 images divided into three categories: diabetic, AMD and healthy subjects. The ground truth ONH boundaries are manually delimited by trained experts [32-35].

3. Performance evaluation

To perform an objective assessment of the outputs of an algorithm for image processing, quantitative metrics have been proposed. These measurements allow comparison of the outcome of a feature extraction method, with a reference standard, in order to perform its validation [36].

Algorithms used in feature extraction techniques, such as segmentation or object location, work on the image's pixels. Therefore, the rules used to classify pixels in terms of pertinence to an object or not, generate four possible classification outcomes. True positive (TP) and True Negative (TN) denote a pixel correctly identified as part of the object or the non-object, while False Positive (FP) and False Negative (FN) denote the pixels incorrectly classified. We note that this approach, which is well suited to the fine granularity of pixel data, does not equate to the retrieval of the subtended information content performed by a clinician. Therefore, starting from this pixel-classification, several mathematical and statistical measures of the performance of an image processing algorithm can be employed.

At present, our review has not identified any uniformity amongst the researchers beyond a quantification in terms of pixels being correctly attributed to specific features [33,37,38].

All the diverse techniques found during this literature review are therefore individually detailed in Table 2.

4. Current Status of Features-based techniques

In this review, we are dealing specifically with the recent feature-based techniques that exploit the visual (morphological, spectral) characteristics of the objects. Therefore, we have divided the

approaches to retinal object segmentation, according to the feature involved. A summary of anatomical feature techniques and outcome results reviewed can be found in Table 3.

4.1 Anatomical Structures

Optic Nerve Head - The OD size, together with cup morphology, and its relationship with the total disc margin is particularly important in the context of glaucoma disc grading. The *neuroretinal rim* describes the margin between disc cup circumference and total disc circumference, comprising the retinal nerve fiber axons. Loss of these axons underpins the pattern of field loss observed in glaucoma. The OD typically presents on a fundus image as a bright circle or ellipse with yellow or white coloring [39] and is usually identified from the red channel of an image due to the highest contrast difference with the background retina [40,41]. The location of the OD can be used as a reference point to establish the position of the macula on the fundus image [42]. The OC is observed as a brighter circular feature within the OD area, as shown in Figure 1, which can be segmented using the green channel where a high level of contrast is observed [43].

There are many well-documented techniques to localize and segment the OD such as using image contrast and brightness [44,45], deformable model [42], principal component analysis [46] and pyramidal decomposition and template matching [38]. The methods reviewed in this paper describe some of the more recent techniques that extend or continue the existing published work as reviewed by Mookiah *et al.*, Haleem *et al.* and Raja *et al.* [38,47,48] focusing on robust methods that accurately identify boundaries of the OD and OC for automatic computer-assisted feature detection and diagnosis of pathologies.

To improve robustness when identifying the OD or OC boundary, adaptive filters have been implemented by Issac *et al.* [43] and Dashtbozorg *et al.* [24]. These segmentation techniques can adapt the filter applied to the image, independently from the image spatial resolution and field of

view (FOV). This enabled their segmentation techniques to be applied to a much larger range of images for validation, prospectively simplifying implementation into a real clinical environment.

An advancement in using image brightness to segment the OD and OC was demonstrated by Issac *et al.* [43] with the aim of improving automatic glaucoma classification. Statistical measures such as the mean and standard deviation of pixel intensities are used to determine an adaptive threshold, to identify OD and OC boundaries. The main advantage of this technique was its invariance to the quality of the image and the noise content, providing a more robust segmentation for cup to disc ratio measurements. Glaucoma detection results found this technique to be 94.4% accuracy (Acc) with 100% sensitivity (Se) and 90% specificity (Sp), performed on a local database of 67 images. Dashtbozorg *et al.* recently demonstrated an adaptive automated OD segmentation, focusing on providing meaningful results in images that contain severe pathological evidence [24]. Classified as a template matching method (finding elements of an image that match a template), a sliding band filter (SBF) was used which enhanced bright regions of the image, implemented in locating the OD center and boundary. Blood vessels were removed from the images and a low-resolution SBF was applied to the fundus image to initially locate the OD center. A second adaptive high-resolution SBF is applied to the image once the OD center has been found, to isolate the OD boundary, which was segmented and smoothed. This method was proven to demonstrate better detection results in comparison to recently published techniques, with an Acc of 99.9% and 99.6% on the MESSIDOR and INSPIRE-AVR databases respectively. However, it was noted that if the initial center detection phase was incorrect, the OD detection was more likely to fail.

Evidence of pathology or poor initial image acquisition can give rise to images with artifacts or poorly defined object boundaries. These artifacts cause problems when trying to segment the OD or OC as a specific boundary is sought out from the image using a variety of different image characteristics. Development of segmentation methods by Dashtbozorg *et al.* [24] and Mookiah *et al.* [49] were focused on identifying boundaries. Mookiah *et al.* used Attanassov intuitionistic fuzzy histon

segmentation to identify a fuzzy or unclear boundary. This method was found to identify the OD boundary with 93.4% Acc and an F-score of 0.92 on 100 images, without any shape constraints being applied on healthy, DR and Glaucoma cases. This study compared results with other conventional histogram based segmentation techniques (Otsu [50] and Gradient Vector Flow [51]) and was found to be superior at detecting unclear OD boundaries.

Another technique adapted to improve the accuracy of OD boundary segmentation is to implement prior knowledge into the computer processing. Prior knowledge based on anatomical features of the retina was implemented by Cheng *et al.* [52] and Basit and Fraz [53]. Cheng *et al.* used superpixels which are local and coherent regions of pixels that are clustered together as they contain similar features, allowing one to differentiate the OD region from the peri-papillary atrophy by comparing the textures of the two anatomical structures [52]. They classified pixels as either disc or non-disc and then applied a deformable body to identify the contour boundary. To identify the OC boundary prior knowledge has been incorporated by applying a region of interest (ROI) from the segmented OD, reducing the area in which superpixels are classified as cup or non-cup pixels. One limitation of this method was the trained classifier used for cup segmentation was dominated by medium sized cups, and therefore underestimation of very large cups, and overestimation of small cups was observed. This method for OD and OC segmentation achieved an area under the curve (AUC) of 0.800, 0.039 lower than the manual disc and cup boundary determination. Basit and Fraz [53] focused on accurate detection and extraction of the OD region by ensuring that OD detection is as specific as possible. The OD center was detected using knowledge that the OD appears as a bright spot and therefore contains maximum intensity pixels. Initially, the main blood vessels were extracted and removed. Regions of maximum pixel intensity were found and underwent further classification to specifically differentiate the OD from other bright spots. The constraints applied for differentiation took into account existing knowledge of the OD and restricted the candidate region to not be at the image boundary, and that a main vessel was found in the neighborhood of the

candidate region. Any maxima that were isolated that did not meet the constraints applied were deleted. Once the region was correctly isolated, a region-based segmentation (watershed transform) was applied to segment the OD boundary. This method reported results of an average OD detection Acc of 98.9% with an average Sp and Se of 99.2% and 76.2% respectively for SHIFA (local database), DRIVE and CHASE_DB1 and DIARETDB1. However, this method had limitations that if the vessels were not extracted accurately or the OD did not contain a region of maximum intensity, the location constraints could not be applied and the initial detection phase failed.

Reza *et al.* [54] looked to significantly reduce the computer processing time of each image by automatically detecting the OD region using a curve operator, inspired by the work performed by Lu and Lim [55]. The benefit of this method was that by not having to apply a background mask or segment the vessels, the processing time per image was reduced, which would enable a higher throughput of data when used in computer-aided diagnosis. The curve operator was fast and efficient for OD region detection, at the expense of boundary detection accuracy. This compromise may not be necessary as Welfer *et al.* [56] achieved a detection Acc of 97.7% taking 7.89s per image on DIARETDB1 in comparison to the reported 94.4% in 6.13s per image using this technique. The curve operator of Reza *et al.* located the ROI by searching for a circular area that was either brighter or darker than the background pixels, and further specified the correct region by selecting a region that contained a gradient of color or pixel intensity across the OD area from the temporal edge (brighter) to the nasal edge (darker). A limitation of this method was that the curve operator failed if the OD region is not distinguishable from the background in terms of pixel intensity as this technique relies on the concept that the OD is either notably brighter or darker than the background.

Blood Vessels - Retinal blood vessels, along with the ONH, are one of the clearest and most well-defined objects in a fundus image. Therefore, their segmentation is used not just to detect pathologies directly connected to the retinal vascular structures, but also as landmarks for several position detection and registration techniques [57-59]. The retinal blood vessels network originates

from the central retinal artery, that arise out of the center of the ONH and spread all over the retina surface forming, along with its three layers of capillary network, a tree-shape structure [60], as shown in Figure 2. The quantitative analysis and classification of the architectural features of this tree-like network allows the monitoring and detection of several pathologies. In DR, for instance, high blood sugar level and ischemia can alter the natural elasticity of the inner walls of the vessels, especially in small capillaries, creating bulges and new vessels in the late proliferative stage. Measuring the *width (cross-section diameter)*, *tortuosity (relative curvature*), *branching morphology (angle and coefficient)* and *fractal dimension* of the vasculature allows the detection of blood filled dilatations, called microaneurysms, and of new vascularization [59,61-63]. Changes in these biomarkers can also be statistically related to hypertension, obesity, cardiovascular disease, cerebrovascular diseases and stroke, increasingly common conditions globally [64-68]. The classification of the blood vessels into arteries and veins can be obtained by the *intensity level* and *color* information extraction [69,70].

To isolate an element of the image with a characteristic intensity level, a good preliminary strategy is to identify the color channel with the highest contrast between that element and the other retinal structures and apply a threshold. Unfortunately, in images with pathological features or in the presence of artifacts and noise, this method produces a runaway number of FP and FN. To target the segmentation process specifically on blood vessels it is necessary to make a step forward and develop a method able to exploit morphological features.

Retinal vessels can easily be distinguished among the set of objects that lie on the ocular fundus image by their piecewise linear shape, the tree-shape branching and the decrease in diameter as they move radially outward from the OD.

A matched filter exploits the abovementioned features along with the assumption that the cross-sectional pixel intensity profile of the vessels has a Gaussian-like profile [71,72]. An example has

been proposed by Odstrcilik *et al.* [19]. Here, a contrast enhancement algorithm was applied to the green channel, where the contrast between vessels and other structures is maximal. This algorithm equalizes the non-uniform illumination of the fundus image and increases the contrast of those structures with an intensity level very different from the background (vessels, exudates and hemorrhages). After this pre-processing step, five different filters, with a Gaussian-like profile, were applied to extract the vasculature, designed to cover the blood vessel width range. The final binary representation of the vascular tree was then obtained by thresholding the histogram and removing the unconnected objects. This method was tested on the DRIVE, STARE and the HRF database. The Se and Sp were 78.5% and 95.1% respectively for the first two databases with an Acc of 93.4%, and 79.0% and 97.5% respectively for the HRF database with an Acc of 97.4%.

A line detector not based on the Gaussian profile of the vessel was designed by Nguyen *et al.* [73]. Here, an optimized line detector was used to detect the vessels. The common limits of this technique, that includes FPs at regions close to strong vessels and the merger of nearby vessels, have been partially overcome by combining two different approaches. First, by reducing the length of the aligned lines of the detector, avoiding the inclusion of adjacent vessel pixels. Secondly, background noise was reduced by increasing the dynamic range of the intensity levels of the pixels using a local contrast enhancement. The resulting effect was tested on the DRIVE and STARE databases, with an Acc of 94.1% and 93.2% respectively.

Akram and Khan used a 2-D Gabor wavelet to enhance vascular structures and thin vessels [74]. This directional selective algorithm has the double advantage of filtering out background noise and adjusting its detectability level by tuning the spatial frequency of the wavelet. The result of this enhancement was used as an input for multi-layered thresholding. In this last stage, several levels of threshold values and validation masks were applied with different rules, eliminating false edges and generating a binary map of the blood vessels. This technique obtained good results in DRIVE and STARE, with an Acc of 94.7% and 95.0% respectively.

To avoid the issues related to the learning process of image classifiers (learning rate, learning epoch and local minima) Bala and Vijayachitra implemented an Extreme Learning Machine classifier [75]. An Extreme Learning Machine is a feedforward neural network used to handle problems difficult to solve with classical parametric techniques [76]. In particular, the authors chose to employ a three-step single hidden layer feedforward neural network. This artificial network has three layers (input, hidden and output) of interconnected nodes that mimics the neurons in a brain. The features used to train this neural network were extracted from the pre-processed retinal image (histogram equalization and segmented by a matched filter). Among the features extracted and used to classify retinal images there are some first and second order statistical texture values, such as entropy, energy, correlation and homogeneity. The method was tested on DIARETDB0 and DRIVE databases obtaining a Se of 96.7% and 100%, Sp of 100% and 94.1% and an Acc of 97.5% and 95.0% respectively. Neural networks have also been used by Liskowski and Krawiec [77], who designed a pre-trained convolutional neural network for vascular segmentation. This multi-layer approach, based on the succession of convolutional, pooling and fully connected layers, has been applied on STARE and DRIVE datasets achieving an Acc up to 97.0% and 95.1% respectively.

Azzopardi *et al.* adopted a strategy that aimed to automatically segment vessel trees in low quality retinal images [78]. In the pre-processing stage, several algorithms were applied to smooth the strong contrast around the circular border of the FOV area and to enhance the overall contrast of the fundus image. The smoothing technique, developed by Sores *at al*. [79], performs dilation of the border, replacing every black pixel with the mean value of its neighbors inside the ROI. This process was repeated several times, augmenting the radius of the ROI by one pixel per iteration. The enhancement was achieved using a histogram equalization algorithm developed by Pizer *at al*. [80]. The actual segmentation, based on a computational model called bar-selective combination of shifted filter responses (B-COSFIRE), employed some difference-of-Gaussian filters to detect the

change of intensity typical of a vessel-object. Of particular interest is the design of different difference-of-Gaussian functions, an excitatory one and an inhibitory one, that simulate the behavior of some groups of cells in the lateral geniculate nucleus of the visual path. This trainable filter has shown to be computationally efficient. By tuning the values of the blurring and shifting operators, used to increase its detectability property, B-COSFIRE filter was able to detect vessels in different orientation and the end of the vessel. Tests on DRIVE, STARE and CHASE_DB1 obtained values of Se and Sp up to 77.2% and 97.0% respectively.

A segmentation technique that doesn't require any pre-processing or training was devised by Wang *et al*. [81]. To create the binary map of the vessel tree the authors combined a novel vessel enhancement method, based on the matched filters with multiwavelet kernels, and a multiscale hierarchical decomposition as a vessel locator. To achieve the first task, the filters that better match the multimodal profile of the vessels, caused by their central specular reflection, were selected. The filter was applied to the image at several orientations in order to find the maximum, hence the profile of the vessel. This multiscale hierarchical decomposition technique allows the detection of the vessels and the reduction of the noise at the same iteration. This is possible through the minimization of the total variation function which decomposes the image into two components, namely; the part that contains the features of interest and a part related to the noise. The ability of this algorithm to identify small features without confusing them with noise is the main goal of this strategy. An adaptive thresholder is then applied to obtain the binary map. The quantitative analysis of this technique conduced on DRIVE and STARE datasets revealed an Acc of 94.6% and 95.2% respectively.

4.2 Macula and Fovea

The central area of the retina is the macula (*macula lutea)*, measuring 5.5mm diameter, the macula exhibits an oval shape, centered between the vascular arcades and OD. Moving from the peripheral

towards the central region of the retina, a dramatic change in the distribution of the photoreceptors (cones and rods) is observed. While the density of rods radially decreases, the cones density reaches its peak. When dissected from the underlying choroid, the macula has a yellow appearance owing to xanthophyll pigments. This protective pigmentation produces a gradual darkening appearance clearly visible in the digital retinal image. The central 1.5mm of the macula comprises the fovea (*fovea centralis)*, which is caters for high spatial acuity and color vision. The *foveola* is the central 0.35mm diameter region where the cone photoreceptors are most densely packed. The central 150 micron depression within the foveola is called the *umbo*. A region within the fovea devoid of blood vessels is the *foveal avascular zone*. The center of this area is considered the center of the macula, and the focus of fixation.

Locating the position of the macula and fovea is crucial in the automatic detection of pathology related to diabetes, such as diabetic maculopathy. If disease in this area becomes chronic, damage to the composite photoreceptors becomes irreversible [82]. There is increasing evidence that as the surviving diabetic population ages, blindness secondary to maculopathy exceeds that of proliferative retinopathy [83].

As observed from the literature, most of the techniques used to locate the ROI containing the macula rely on some anatomical assumptions related to the distance between the fovea and OD [46,58,84,85]. The exact location of the fovea is achieved by various algorithms, such as thresholding or template matching, usually preceded by a filtering stage where blood vessel abnormalities are removed.

An example of this procedure was presented by Chin *et al*. [86]. To locate the fovea center the authors combined the information provided by the vessels and OD segmentations with some a-priori knowledge about the anatomical structure of the retina. To establish the search area, the vessel arch was used as template to draw a hypothetical parabola with a vertex on the nasal side of the OD. The

search interval was selected along the principal meridian of this parabola at a specific distance from the disc, in terms of disc diameter (DD). Such distance was estimated calculating the disc-macula distance from a sample of 126 images. Inside this area, the window with the minimum number of vessel pixels was considered as fovea. To measure the performance of this method the number of correct detections (NCD) within 25%DD and 50%DD was performed. MESSIDOR and some images from the Tayside diabetic screening program at Ninewells Hospital (Dundee) were used to validate the technique. The performance were better on the latter, with a NCD-25% of 51/66 and a NCD-50% of 61/66 in high resolution images.

To overcome the time consuming process of blood vessel segmentation and vascular arch parabola fitting, Zheng *et al*. developed a technique based on anatomical structure constraints and their relative location, and on intensity level information related to the OD [87]. In the pre-processing stage a course localization of the OD was performed analyzing the intensity levels of red channel of the retinal image. After the elimination of the blood vessels, the OD boundary was detected using a region-based model [88]. From this boundary a circle was fitted to obtain the position and radius of the OD. This information was used to provide constraints in order to narrow the search area for the fovea. To locate the temporal side of the OD the brighter area was detected, the side less covered by blood vessels. To this side, the distance of 2.5 OD diameter off the center of the OD and 5-degree below, referred to the x axis of the image, was selected as research area. The final position of the fovea was then detected by applying a morphological geodesic reconstruction [89]. This allows the removal of all the undesirable features, such as bright spots, vessels and so on. The outcome is a connected area with constant intensity level. The geometrical center of this area is the fovea center. This method was performed on DRIVE, obtaining a detection success rate of 100%, on HEI-MED obtaining 98.8% and DIARETDB1 with 93.3%.

An extraction method independent from geometrical relationship estimation and blood vessel removal was described by Medhi and Dandapat [82]. In this work the color intensity normalization

and the contrast enhancement of the retinal image in the pre-processing stage involved the use of different color spaces. The first color normalization took place in the luminance plane of YIQ color space, where the Y plane was modified according to a specific parametric rule proposed by Sánchez *et al*. [90]. A second transformation was applied on the HIS color space. To detect the circular region containing the macula the authors used two sets of information: the absence of blood vessels and the location of the OD. Because the superior and the inferior arteries of the retina are arranged horizontally with respect to the macula in a fundus image, a horizontal canny edge detector was used to find them. Within the central region between these arteries, the macula and fovea were located. The intensity value was then inverted and the binary image of the macula region obtained through an Otsu's thresholding. A further Hough transformation was applied to the edges of the macula in order to define the circular geometry of the macula and its center, the fovea. A well-established way to evaluate the performances of macula detection methods is to measure the Euclidean Distance between the manual segmented image and the one processed by the feature extractor algorithm [83]. The analysis was performed on DRIVE and DIARETDB1 datasets obtaining an average distance of m=6.88 pixel and a standard deviation of s=5.85 pixel in the first and m=8.90 pixel and s=12.89 pixel in the second.

4.3 Abnormalities

Observed abnormalities that indicate disease can be separated into three categories when analyzing an image: bright lesions, dark lesions and new vessels [91], in Figure 3 a broad overview is shown. Pathological features represented by bright lesions are exudates (lipoproteins) and cotton wool spots (superficial retinal infarcts). Microaneurysms and hemorrhages (dot, blot and flame) are examples of dark lesions. New vessels are dark features that can be detected due to the fact they do not take paths of known non-pathological retinal vessels. For detection and classification of abnormalities, the principles used to identify known anatomical structures of fundus images are

modified to optimize the detection of each lesion type. A list of the techniques and outcome results for abnormalities can be found in Table 4.

Bright Lesions – Automatic screening for DR and AMD requires the detection and segmentation of abnormal bright lesions so that the disease progression can be interpreted [34,35,92,93]. Bright lesions appear as blob-like structures characterized by varying levels of intensity, often appearing as the features in the retinal image with the highest absolute luminance [93].

Zhang *et al.* [92] detected exudates on retinal images with the aim of improving retinal screening for DR by automatically identifying normal exams in a tele-medicine network. This was the first reported method to identify and classify reflections and artifacts during the pre-processing stage, preventing their inclusion in the subsequent manual exudate identification process. Regions of known brightness on an ocular fundus image, such as the OD, bright regions at the border and the FOV contour are removed to isolate abnormal bright regions. These bright regions underwent a classification process to identify exudates from the known variability in shape and contrast of exudates. This method for exudate segmentation and classification produced an AUC of 0.950 when validated on the e-ophtha EX database.

Mookiah *et al.* [34,35] have recently published two different methods to classify images as normal or as containing AMD. The main advantage of both of these methods is that no prior segmentation of lesions and anatomical structures was required. In [34] potential exudates were detected by analyzing changes in texture properties by looking at regions of pixels rather than individual pixel values. Statistical ranking was performed in order to classify whether the image was normal or AMD was present. In [35] lesions are detected due to the change they cause in spatial orientation and color intensity of fundus images. Empirical mode decomposition detects these non-linear changes in pixels and decomposes the data into a small number of components. These components were then classified to determine whether AMD was present in the image or not. Empirical mode

decomposition has been used to analyze biomedical signals previously [94], however this is the first reported use applied to AMD detection. In [34], results were reported with an Acc of 97.6% and 90.68% on the STARE and ARIA databases respectively whereas [35] reported results of 100% Acc for STARE and 85.1% Acc for ARIA when classifying the presence of AMD. Both techniques were therefore suggested to be suitable for AMD clinical screening.

Dark Lesions – Figueiredo *et al.* [95] developed an automated system for the classification of DR lesions such as, microaneurysms, hemorrhages and bright lesions using suitable binary classifiers. Analysis of several wavelet bands, thresholding and segmentation are used to retain relevant and remove redundant information. This process was repeated at multiple stages for optimal detection of each lesion type dependent on its intrinsic properties. Validation of the automated system was performed on the HEI-MED, MESSIDOR, DIARETDB0 and DIARETDB1 databases along with private databases provided by retinal specialists. Detection performance for microaneurysms was 93% Se and 89% Sp, hemorrhages was 86% Se and 90% Sp and bright lesions was 90% Se and 97% Sp. When considered together as an automated screening system for DR, an average of 95-100% Se and 70% Sp were achieved.

Seoud *et al.* [96] demonstrated a method, aimed at automated tele-medicine detection and severity grading of DR, which was able to differentiate microaneurysms and hemorrhages without specific segmentation of each feature. Microaneurysms were distinguished from hemorrhages by the shape characteristics of each lesion, microaneurysm being determined to be a small red dot whilst a hemorrhage was more likely to be represented by an elongated red structure. Using this prior knowledge of how each lesion presents on an image, potential lesions were detected using thresholding and classified using dynamic shape features (region classification based on shape) to differentiate false positives from true lesions rather than template matching. The advantage of this technique is that prior vessel segmentation is not required, the types of red lesions can be differentiated from one another, and classification of images containing pathology is good (based on

red lesions only) as only one lesion was needed to be detected to infer the presence of pathology. However, severity grading may be currently insufficient in the current implementation due to the difficulty in distinguishing between normal and DR1 images.

5. Expert commentary

The prospect of obtaining reliable clinical software for the assessment of fundus images is becoming more and more solid. The significant amount of retinal images made publically available is one of the key factors in determining this trend. In particular, the publication of databases with different pathological signs, graded by experts, is allowing research groups to validate and compare their techniques. Nevertheless, there are two main issues that must be addressed in automatic retinal image analysis: the quality of fundus imaging (level of resolution, uniformity, dynamic, noise and artifacts) and the alteration of the information content caused by the image processing itself. If the first one is going to be overcome by the constant improvement and spread of high quality image sensor technology, the second one will still remain a trade-off [37,38,47].

The basic concept of using an algorithm to detect a feature inside a 2D matrix of pixels is based on the definition of rules that act on the digital data features, rather than on the anatomical feature itself. Therefore, in order to design the algorithmic constraints, researchers are commonly induced to consider the “digital characteristic” of the retinal object (intensity level and spatial position of the pixels), rather than its clinically relevant information. The result is that the effectiveness of this approach is strongly influenced by the quality and the variability within the digital features, for example those caused by different environmental conditions, differences between subjects and instrumentation.

Filtering techniques with few constraints, like model-based and matching methods, may not be robust enough to consider this high variability. On the other hand, supervised algorithms may require several levels of rules and large amounts of data to be trained. The pre-processing stage

used to partially overcome this variability, enhancing specific characteristics of the digital image, does not take into consideration the loss of information content caused by this data-transformation. This aspect is hardly ever considered in the works reviewed but could play a role in the identification of the clinically relevant information within the retinal image.

The performance, in terms of sensitivity and specificity attained by the automated grading software considered in this paper, show values well above 90%. However, absolute values of these are difficult to interpret when deciding whether an algorithm would perform effectively within a screening program [97]. Such feature-based validation procedures are necessary for the assessment of automatic grading systems suitability for clinical adoption. The societal and economic benefits of this would be profound.

6. Five-year view

The urgency of reducing avoidable blindness and visual impairments in low- and middle-income countries has been highlighted by the WHO [3,4]. A promising strategy able to overcome the lack of general practitioners and infrastructure is offered by automatic retinal image analysis [1,2]. Even in high-income settings, where DR and maculopathy are significant [3], this technology may facilitate and accelerate the population screening procedure and reduce costs. For example, an analysis by Scotland et al. found that a national automated screening program for DR in Scotland ought to cost 230,400 GBP for 160,000 patients, representing savings of over 200,000 GBP compared to its manual counterpart [98]. Furthermore, the diffusion of everyday devices able to speed up this process, such as smartphones [6,7], is challenging researchers to deliver a reliable and robust system for automatic grading of retinal imaging.

The adoption of machine learning algorithms and neural networks for pattern recognition and classification is a strategy increasingly taken into account by the research community, as highlighted by the volume of related presentations at 2015 IEEE EMBC, producing promising results. The natural

propensity of these data processing algorithms for dealing with a high variability of data and their recognition of relevant medical features through a training process, is something very close to the cognitive process employed by a physician. The public availability of retinal datasets is boosting this process and challenging the researchers to deal with large-scale unstructured medical images. Research enhanced by Google Deep Mind could produce promising developments in this area [99].

As the technology of image sensors are developed over the next 5 years, this quantity of data is set to increase, including high-resolution images, less affected by noise and artifacts. Furthermore, its diffusion worldwide will allow to achieve a wide range of pathological variability.

The approval of automated grading systems within population-wide screening programs [97] has been the result of a direct comparison between the manual and automatic detection rate in different clinical environments. However, the current validation assessment is based on parameters usually employed in the digital image processing field. Although this approach was justified by the connection between the digital information of the fundus image and its processing, a better definition of the clinical information content of the retinal image is expected over the next few years, along with a better description of the performance evaluation.

7. **Key issues**

- Screening programs are fundamental in preventing and identifying treatable pathologies, which account for 80% of the global number of blind people.
- The assessment of retinal images is a time consuming process that requires fragile instrumentation, related logistics and infrastructure, and the presence of a trained person, conditions difficult to achieve in low- and middle-income countries.
- The development of community-specific retinal imaging solutions, such as mobile phone technology for mHealth, and the increase in quality and diffusion of imaging technology promise to overcome the problem of obtaining affordable high-quality retinal images.

- To deal with the high number of fundus images thus generated, researchers are developing several strategies for automatic and semi-automatic systems.
- The definition of links between clinically relevant information and the digital information within the image's pixels is the key aspect in integrating the feature assessment process, employed by clinicians, into an algorithmic process.
- For different retinal features, different techniques are adopted, highlighting the specificity of the digital information used to evaluate different parameters.
- Training and validation processes for algorithms are made more easily accessible by the diffusion of publicly available databases.
- The evaluators used to compare the algorithmic performance are not immediately interpretable when defining their usability in screening program.
- The rapid diffusion of these software into clinical setting, over the next 5 years, will provide a new definition of performance and a better understanding of clinically relevant information in digital imaging.

Funding

The work has been funded by the University of Strathclyde and the Queen Elizabeth Diamond Jubilee Trust.

Declaration of interest

The authors have no relevant affiliations or financial involvement with any organization or entity with a financial interest in or financial conflict with the subject matter or materials discussed in the manuscript. This includes employment, consultancies, honoraria, stock ownership or options, expert testimony, grants or patents received or pending, or royalties.

References

Papers of special note have been highlighted as:

• of interest

•• of considerable interest

1.Prince JL, Links JM. Medical imaging signals and systems. Upper Saddle River (NJ): Pearson Prentice Hall; 2006.

2.Foster KR, Koprowski R, Skufca JD. Machine learning, medical diagnosis, and biomedical engineering research-commentary. Biomed Eng Online. 2014;13:1.

3.World Health Organization. Universal eye health: a global action plan 2014-2019. 2013.

4.Pascolini D, Mariotti SP. Global estimates of visual impairment: 2010. Br J Ophthalmol. 2012;96:614-8.

5.Chatziralli IP, Kanonidou ED, Keryttopoulos P, et al. The value of fundoscopy in general practice. Open Ophthalmol J. 2012;6:4-5.

6.Bolster NM, Giardini ME, Livingstone IA, Bastawrous A. How the smartphone is driving the eye-health imaging revolution**.** Expert Rev Ophthalmol**.** 2014;9:475-85.

7.Kay M, Santos J, Takane M. mHealth: New horizons for health through mobile technologies. World Health Organization. 2011;64:66-71.

8.Gonzalez RC, Woods RE. Digital Image Processing. 3rd ed. ed. Upper Saddle River(NJ): Pearson Prentice Hall; 2008.

9.Winder RJ, Morrow PJ, McRitchie IN, et al. Algorithms for digital image processing in diabetic retinopathy. Comput Med Imaging Graph. 2009;33:608-22.

10.Besenczi R, Tóth J, Hajdu A. A review on automatic analysis techniques for color fundus photographs. Comput. Struct. Biotechnol. J, 2016;*14*,:371-384.

11.Carmona EJ, Rincon M, Garcia-Feijoo J, Martinez-de-la-Casa JM. Identification of the optic nerve head with genetic algorithms. Artif Intell Med. 2008;43:243-59.

12.Fumero F, Alayon S, Sanchez JL, et al. RIM-ONE: An Open Retinal Image Database for Optic Nerve Evaluation. Comp Med Sy. 2011:1-6.

13.Staal J, Abramoff MD, Niemeijer M, et al. Ridge-based vessel segmentation in color images of the retina. IEEE Trans Med Imaging. 2004;23:501-9.

14.Shanmugam V, Banu RSDW. Retinal Blood Vessel Segmentation using an Extreme Learning Machine Approach. 2013 IEEE Point-of-Care Healthcare Technologies (PHT). 2013:318-21.

15.Gurudath N, Celenk M, Riley HB. Machine Learning Identification of Diabetic Retinopathy from Fundus Images. Signal Processing in Medicine and Biology Symposium (SPMB), 2014 IEEE. 2014:1-7.

16.Al-Diri B, Hunter A, Steel D, et al. REVIEW - a reference data set for retinal vessel profiles. Conf Proc IEEE Eng Med Biol Soc. 2008;2008:2262-5.

17.Fraz MM, Remagnino P, Hoppe A, et al. An ensemble classification-based approach applied to retinal blood vessel segmentation. IEEE Trans Biomed Eng. 2012;59:2538-48.

18.Owen CG, Rudnicka AR, Mullen R, et al. Measuring retinal vessel tortuosity in 10-year-old children: validation of the Computer-Assisted Image Analysis of the Retina (CAIAR) program. Invest Ophthalmol Vis Sci. 2009;50:2004-10.

19.Odstrcilik J, Kolar R, Kubena T, et al. Retinal vessel segmentation by improved matched filtering: evaluation on a new high-resolution fundus image database. IET Image Processing. 2013;7:373-83.

20.McCormick B, Goldbaum M. STARE= Structured Analysis of the Retina: Image processing of TV fundus image. Jet Propulsion Laboratory, Pasadena, CA: USA-Japan Workshop on Image Processing 1975.

21.Hoover A, Goldbaum M. Locating the optic nerve in a retinal image using the fuzzy convergence of the blood vessels. IEEE Trans Med Imaging. 2003;22:951-8.

22.VICAVR D. 2010 Available from: http://www.varpa.es/vicavr.html. [Last accessed: 28 September 2016]

23.Dashtbozorg B, Mendonca AM, Campilho A. An automatic graph-based approach for artery/vein classification in retinal images. IEEE Trans Image Process. 2014;23:1073-83.

24.Dashtbozorg B, Mendonca AM, Campilho A. Optic disc segmentation using the sliding band filter. Comput Biol Med. 2015;56:1-12.

25.Dashtbozorg B, Mendonça AM, Campilho A. Automatic Estimation of the Arteriolar-to-Venular Ratio in Retinal Images Using a Graph-Based Approach for Artery/Vein Classification. In: Kamel M, Campilho A, editors. Image Analysis and Recognition: 10th International Conference, ICIAR 2013, Póvoa do Varzim, Portugal, June 26-28, 2013 Proceedings. Berlin, Heidelberg: Springer Berlin Heidelberg; 2013. p. 530-8.

26.Grisan E, Foracchia M, Ruggeri A. A novel method for the automatic grading of retinal vessel tortuosity. IEEE Trans Med Imaging. 2008;27:310-9.

27.Kauppi T, Kalesnykiene V, Kamarainen J-K, et al. DIARETDB0: Evaluation database and methodology for diabetic retinopathy algorithms. Machine Vision and Pattern Recognition Research Group, Lappeenranta University of Technology, Finland. 2006.

28.Kauppi T, Kalesnykiene V, Kamarainen J-K, et al. The DIARETDB1 Diabetic Retinopathy Database and Evaluation Protocol. BMVC 2007 September 10

29.MESSIDOR T-V. MESSIDOR: methods to evaluate segmentation and indexing techniques in the field of retinal ophthalmology. 2014. Available from: http://messidor.crihan.fr/index-en.php. [Last accessed: 28 September 2016]

30.Decencière E, Cazuguel G, Zhang X, et al. TeleOphta: Machine learning and image processing methods for teleophthalmology. IRBM. 2013;34:196-203.

31.Giancardo L, Meriaudeau F, Karnowski TP, et al. Exudate-based diabetic macular edema detection in fundus images using publicly available datasets. Med Image Anal. 2012;16:216-26.

32.Medhi JP, Nath MK, Dandapat S, Automatic grading of macular degeneration from color fundus images. Information and Communication Technologies (WICT), 2012 World Congress on 2012 Oct. 30 p. 511-4. IEEE.

33.Mittal D, Kumari K. Automated detection and segmentation of drusen in retinal fundus images. Comput Electr Eng.. 2015;47:82-95.

34.Mookiah MR, Acharya UR, Fujita H, et al. Local configuration pattern features for age-related macular degeneration characterization and classification. Comput Biol Med. 2015;63:208-18.

35.Mookiah MRK, Acharya UR, Fujita H, et al. Automated detection of age-related macular degeneration using empirical mode decomposition. Knowledge-Based Syst. 2015;89:654-68.

36.Trucco E, Ruggeri A, Karnowski T, et al. Validating retinal fundus image analysis algorithms: issues and a proposal. Invest Ophthalmol Vis Sci. 2013;54:3546-59.

•• **Organic description of the key issues of the validation process for retinal image analysis algorithms.**

37.Fraz MM, Remagnino P, Hoppe A, et al. Blood vessel segmentation methodologies in retinal images--a survey. Comput Methods Programs Biomed. 2012;108:407-33.

• **Presents a detailed review about blood vessel segmentation methods with technique classification and performance comparison.**

38.Mookiah MR, Acharya UR, Chua CK, et al. Computer-aided diagnosis of diabetic retinopathy: a review. Comput Biol Med. 2013;43:2136-55.

39.Goldbaum M, Moezzi S, Taylor A, et al. Automated diagnosis and image understanding with object extraction, object classification, and inferencing in retinal images. International Conference on Image Processing, Proceedings - Vol Iii. 1996;3:695-8.

40.Almazroa A, Burman R, Raahemifar K, Lakshminarayanan V. Optic Disc and Optic Cup Segmentation Methodologies for Glaucoma Image Detection: A Survey. J Ophthalmol. 2015;2015:180972.

41.Ren F, Li W, Yang J, et al. Automatic optic disc localization and segmentation in retinal images by a line operator and level sets. Technol Health Care. 2016;24 Suppl 2:S767-76.

42.Lowell J, Hunter A, Steel D, et al. Optic nerve head segmentation. IEEE Trans Med Imaging. 2004;23:256-64.

43.Issac A, Sarathi MP, Dutta MK. An adaptive threshold based image processing technique for improved glaucoma detection and classification. Comput. Meth. Programs Biomed. 2015;122(2):229-44.

44.Sinthanayothin C, Boyce JF, Cook HL, Williamson TH. Automated localisation of the optic disc, fovea, and retinal blood vessels from digital colour fundus images. Br J Ophthalmol. 1999;83:902-10.

45.Walter T, Klein J-C. Segmentation of Color Fundus Images of the Human Retina: Detection of the Optic Disc and the Vascular Tree Using Morphological Techniques. In: Crespo J, Maojo V, Martin F, editors. Medical Data Analysis: Second International Symposium, ISMDA 2001 Madrid, Spain, October 8–9, 2001 Proceedings. Berlin, Heidelberg: Springer Berlin Heidelberg; 2001:282-7.

46.Li H, Chutatape O. Automated feature extraction in color retinal images by a model based approach. IEEE Trans Biomed Eng. 2004;51:246-54.

47.Haleem MS, Han L, van Hemert J, Li B. Automatic extraction of retinal features from colour retinal images for glaucoma diagnosis: a review. Comput Med Imaging Graph. 2013;37:581-96.

• R**eview with a narrow focus on ONH feature extraction for Glaucoma diagnosis. Clear summary tables of each extraction technique provided.**

48.Banadict Raja R, Ravichandran C. Optic Disc Localization Methodologies in Retinal Images: A Review. International Journal of Soft Computing. 2015;10:195-202.

49.Mookiah MRK, Acharya UR, Chua CK, et al. Automated detection of optic disk in retinal fundus images using intuitionistic fuzzy histon segmentation. Proceedings of the Institution of Mechanical Engineers, Part H: Journal of Engineering in Medicine. 2012;227:37-49.

50.Nithya R, Venkateswaran N. Analysis of Segmentation Algorithms in Colour Fundus and OCT Images for Glaucoma Detection**.** Indian J Sci Technol. 2015;8:1-6.

51.Thongnuch V, Uyyanonvara B. Automatic optic disk detection from low contrast retinal images of ROP infant using GVF snake. Suranaree J Sci Technol. 2007;14:223-34.

52.Cheng J, Liu J, Xu Y, et al. Superpixel classification based optic disc and optic cup segmentation for glaucoma screening. IEEE Trans Med Imaging. 2013;32:1019-32.

53.Basit A, Fraz MM. Optic disc detection and boundary extraction in retinal images. Appl Opt. 2015;54:3440-7.

54.Reza MN, Ahmad M. Automatic detection of optic disc in fundus images by curve operator. In Electrical Information and Communication Technology (EICT), 2015 2nd International Conference on 2015 10-12, 2012:143-7. IEEE.

55.Lu S, Lim JH. Automatic optic disc detection from retinal images by a line operator. IEEE Trans Biomed Eng. 2011;58:88-94.

56.Welfer D, Scharcanski J, Kitamura CM, et al. Segmentation of the optic disk in color eye fundus images using an adaptive morphological approach. Comput Biol Med. 2010;40:124-37.

57.Lloret D, Serrat J, López AM, et al. Retinal image registration using creases as anatomical landmarks. Pattern Recognition, 2000 Proceedings 15th International Conference; 2000. p203-6. IEEE

58.Niemeijer M, Abramoff MD, van Ginneken B. Automated localization of the optic disc and the fovea. Conf Proc IEEE Eng Med Biol Soc. 2008;2008:3538-41.

59.Perez-Rovira A, MacGillivray T, Trucco E, et al. VAMPIRE: Vessel assessment and measurement platform for images of the REtina. Conf Proc IEEE Eng Med Biol Soc. 2011;2011:3391-4.

60.Kalloniatis M, Luu C. Visual Acuity. In: Kolb H, Fernandez E, Nelson R, editors. Webvision: The Organization of the Retina and Visual System. Salt Lake City (UT): University of Utah Health Sciences Center; 1995.

61.Archana DN, Padmasini N, Yacin SM, Umamaheshwari R. Detection of Abnormal Blood Vessels in Diabetic Retinopathy Based on Brightness Variations in SDOCT Retinal Images. 2015 IEEE International Conference on Engineering and Technology (Icetech); 2015:196-9. IEEE

62.Devaraj D, Prasanna Kumar SC. Blood vessels segmentation with GUI in digital fundus images for automated detection of diabetic retinopathy. 2014 International Conference on Contemporary Computing and Informatics (IC31); Nov 27 2014:915-20

63.Pourreza HR, Pourreza M, Banaee T. Simple and efficient method to measure vessel tortuosity. Proceedings of the 3rd International Conference on Computer and Knowledge Engineering (Iccke 2013) 2013:219-22.

64.Heneghan C, Flynn J, O'Keefe M, Cahill M. Characterization of changes in blood vessel width and tortuosity in retinopathy of prematurity using image analysis. Med Image Anal. 2002;6:407-29.

65.Leung H, Wang JJ, Rochtchina E, et al. Impact of current and past blood pressure on retinal arteriolar diameter in an older population. J Hypertens. 2004;22:1543-9.

66.Wang JJ, Taylor B, Wong TY, et al. Retinal vessel diameters and obesity: a population-based study in older persons. Obesity. 2006;14:206-14.

67.Wong TY, Klein R, Couper DJ, et al. Retinal microvascular abnormalities and incident stroke: the Atherosclerosis Risk in Communities Study. Lancet (London, England). 2001;358:1134-40.

68.Patton N, Aslam T, Macgillivray T, et al. Retinal vascular image analysis as a potential screening tool for cerebrovascular disease: a rationale based on homology between cerebral and retinal microvasculatures. J Anat. 2005;206:319-48.

69.Abbasi UG, Akram MU. Classification of blood vessels as arteries and veins for diagnosis of hypertensive retinopathy. Computer Engineering Conference (ICENCO), 2014 10th International; 2014 29-30 Dec. 2014:5-9

70.Hamednejad G, Pourghassem H. Retinal Blood Vessel Classification Based on Color and Directional Features in Fundus Images. 2015 22nd Iranian Conference on Biomedical Engineering (Icbme); 2015:257-62

71.Chaudhuri S, Chatterjee S, Katz N, et al. Detection of blood vessels in retinal images using two-dimensional matched filters. IEEE Trans Med Imaging. 1989;8:263-9.

72.Hoover A, Kouznetsova V, Goldbaum M. Locating blood vessels in retinal images by piecewise threshold probing of a matched filter response. IEEE Trans Med Imaging. 2000;19:203-10.

73.Nguyen UTV, Bhuiyan A, Park LAF, Ramamohanarao K. An effective retinal blood vessel segmentation method using multi-scale line detection. Pattern Recognition. 2013;46:703-15.

74.Akram MU, Khan SA. Multilayered thresholding-based blood vessel segmentation for screening of diabetic retinopathy. Eng Comput. 2012;29:165-73.

75.Bala MP, Vijayachitra S. Extraction of Retinal Blood Vessels and Diagnosis of Proliferative Diabetic Retinopathy Using Extreme Learning Machine. J Med Imaging Health Inform. 2015;5:248-56.

76.Huang GB, Zhu QY, Siew CK. Extreme learning machine: Theory and applications. Neurocomputing. 2006;70:489-501.

77.Liskowski P, Krawiec K. Segmenting retinal blood vessel with deep neural networks. IEEE Trans Med Imaging. 2016;35:2369-80.

78.Azzopardi G, Strisciuglio N, Vento M, Petkov N. Trainable COSFIRE filters for vessel delineation with application to retinal images. Med Image Anal. 2015;19:46-57.

79.Soares JV, Leandro JJ, Cesar Junior RM, et al. Retinal vessel segmentation using the 2-D Gabor wavelet and supervised classification. IEEE Trans Med Imaging. 2006;25:1214-22.

80.Pizer SM, Amburn EP, Austin JD, et al. Adaptive Histogram Equalization and Its Variations. Comput Vision Graph. 1987;39:355-68.

81.Wang Y, Ji G, Lin P, Trucco E. Retinal vessel segmentation using multiwavelet kernels and multiscale hierarchical decomposition. Pattern Recognition. 2013;46:2117-33.

82.Medhi JP, Dandapat S. An effective fovea detection and automatic assessment of diabetic maculopathy in color fundus images. Comput Biol Med. 2016;74:30-44.

83. Flanagan DW. Current management of established diabetic eye disease. Eye. 2013;7(2):302-8

84.Sagar AV, Balasubramanian S, Chandrasekaran V. Automatic Detection of Anatomical Structures in Digital Fundus Retinal Images. MVA; 2007:483-6.

85.Welfer D, Scharcanski J, Marinho DR. Fovea center detection based on the retina anatomy and mathematical morphology. Comput Methods Programs Biomed. 2011;104:397-409.

86.Chin KS, Trucco E, Tan LL, Wilson PJ. Automatic fovea location in retinal images using anatomical priors and vessel density. Pattern Recognition Letters. 2013;34:1152-8.

87.Zheng S, Pan L, Chen J, Yu L. Automatic and efficient detection of the fovea center in retinal images. 2014 7th International Conference on Biomedical Engineering and Informatics; 2014:145-50.

88.Joshi GD, Sivaswamy J, Karan K, Krishnadas S. Optic disk and cup boundary detection using regional information. 2010 IEEE International Symposium on Biomedical Imaging: From Nano to Macro; 2010:948-51.

89.Mukhopadhyay S, Chanda B. Multiscale morphological segmentation of gray-scale images. IEEE Trans Image Process. 2003;12:533-49.

90.Sanchez CI, Hornero R, Lopez MI, et al. A novel automatic image processing algorithm for detection of hard exudates based on retinal image analysis. Med Eng Phys. 2008;30:350-7.

91.Patton N, Aslam TM, MacGillivray T, et al. Retinal image analysis: concepts, applications and potential. Prog Retin Eye Res. 2006;25:99-127.

92.Zhang X, Thibault G, Decenciere E, et al. Exudate detection in color retinal images for mass screening of diabetic retinopathy. Med Image Anal. 2014;18:1026-43.

93.Ben Sbeh Z, Cohen LD, Mimoun G, Coscas G. A new approach of geodesic reconstruction for drusen segmentation in eye fundus images. IEEE Trans Med Imaging. 2001;20:1321-33.

94.Pachori RB, Avinash P, Shashank K, et al. Application of empirical mode decomposition for analysis of normal and diabetic RR-interval signals. Expert Syst Appl. 2015;42:4567-81.

95.Figueiredo IN, Kumar S, Oliveira CM, et al. Automated lesion detectors in retinal fundus images. Comput Biol Med. 2015;66:47-65.

96.Seoud L, Hurtut T, Chelbi J, et al. Red Lesion Detection Using Dynamic Shape Features for Diabetic Retinopathy Screening. IEEE Trans Med Imaging. 2016;35:1116-26.

97.Fleming AD, Goatman KA, Philip S, et al. Automated grading for diabetic retinopathy: a large-scale audit using arbitration by clinical experts. Br J Ophthalmol. 2010;94:1606-10

98.Scotland GS, McNamee P, Philip S, et al. Cost-effectiveness of implementing automated grading within the national screening programme for diabetic retinopathy in Scotland. Br J Ophthalmol. 2007, 91:1518-1523

99.Moorfields announces research partnership. July 2016. Available from: http://www.moorfields.nhs.uk/news/moorfields-announces-research-partnership. [Last accessed: 28 September 2016]

•• **Validation and audit of implementing an automated grading system for Diabetic Retinopathy within a clinical setting**

Table 1 - Summary of publicly available databases of fundus images for retinal image analysis

Retinal Image Database	No. of Images	Fundus Camera System	Spatial Resolution (pixels)	Field of View (FOV)	Ground Truth or Expert Grading's
DRIVE (Utrecht Database) - Digital Retinal Images for Vessel Extraction	40	Canon CR5 (Canon Corp., Tokyo, Japan)	768 x 564	45°	Blood Vessel Segmentation
REVIEW - Retinal Vessel Image Set for Estimation of Widths HRIS - High Resolution Image Set VDIS - Vascular Disease Image Set CLRIS - Central Light Reflex Image Set KPIS - Kick Point Image Set	16	HRIS - Canon 60 UV VDIS - Zeiss fundus camera CLRIS - Zeiss FF 450 (Carl Zeiss AG, Oberkochen, Germany) KPIS - Canon 60 UV (Canon Corp.)	HRIS - 3584 x 2438 VDIS - 1360 x 1024 CLRIS - 2160 x 1440 KPIS - 3300 x 2600	HRIS - 60° VDIS - 50° CLRIS - 50° KPIS - 60°	Blood Vessel Segmentation
CHASE_DB1 - Child Heart and Health Study in England	28	Nidek NM-200-D (Nidek Co., Ltd., Gamagori, Japan)	1280 x 960	30°	Blood Vessel Segmentation
HRF - High Resolution Fundus Image Database	45	Canon CF-60 Uvi Canon EOS 20D (Canon Corp.)	3504 x 2336	60°	Blood Vessel Segmentation - Optic Disc (OD) detection (center and radius)
STARE - Structured Analysis of the Retina	81	TopCon TRV-50 (Topcon Corp., Tokyo, Japan)	700 x 605	35°	Blood Vessel Segmentation - Artery/Vein Labelling
VICAVR	58	TopCon camera NW-100 (Topcon Corp.)	768 x 584	-	Vessels Caliber - Artery/Vein Labelling
INSPIRE- AVR	40	Zeiss Fundus Camera (Carl Zeiss AG)	2392 × 2048	30°	Artery/Vein labelling - OD Segmentation
BioImLab	60	TopCon TRC-50 (Topcon Corp.)	1300 x 1100	50°	Vessels Tortuosity Evaluation
DRIONS-DB - Digital Retinal Images for Optic Nerve Segmentation Database	110	35mm Film Colour Fundus Camera Digitised using HP-PhotoSmart-S20 scanner (HP, Palo Alto, CA, USA)	600 x 400	-	OD Segmentation
RIM-ONE	159	Nidek AFC-210 (Nidek Co., Ltd.) Canon EOS 5D (Canon Corp.)	2144 x 1424 (stereo images)	-	OD and Optic Cup Segmentation
ImageRet	219	Digital Fundus Camera - Settings Unknown	1500 x 1152	50°	Diabetic Retinopathy (DR) Lesions Grading
MESSIDOR	1200	TopCon TRC NW6 (Topcon Corp.)	1440 x 960 or 2240 x 1488 or 2304 x 1536	45°	DR Grading - Macula Edema Risk Level
E-Ophtha	463	Telemedical Network Various Cameras used	EX (2048 x 1360 and 1440 x 960) MA (1440 x 960 and 2544 x 1696)	-	DR Lesions Grading
HEI-MED - Hamilton Eye Institute Macular Edema Dataset	169	Zeiss Visucam PRO fundus camera (Carl Zeiss AG)	2196 × 1958	45°	-
ARIA - Automated Retinal Image Analysis	450	Zeiss FF450+ Fundus Camera (Carl Zeiss AG)	768 x 576	50°	Optic Nerve Head boundary segmentation

Table 2 - Performance Evaluators – Statistical measures mostly used for the evaluation process of feature extraction methods.

Measure	Description	Formula
Sensitivity (Se) or True Positive Fraction (TPF) or Recall (Rec)	The proportion of pixels that are correctly identified as object	$\frac{TP}{TP + FN}$
Specificity (Sp) or True Negative Fraction (TNF)	The proportion of pixels that are correctly identified as non-object	$\frac{TN}{FP + TN}$
Precision or Positive Predicted Value (PPV)	The proportion of positive results that are true positive	$\frac{TP}{TP + FP}$
Negative Predicted Value (NPV)	The proportion of negative results that are true negative	$\frac{TN}{TN + FN}$
Accuracy (Ac or Acc)	It describe the closeness of a measurement to the true value	$\frac{TP + TN}{TP + FP + FN + FN}$
False Positive Fraction (FPF)	The proportion of pixels that are not correctly identified as object	$\frac{FP}{TP + FN}$
False Negative Fraction (FNF)	The proportion of pixels that are not correctly identified as non-object	$\frac{FN}{TP + TN}$
Receiver Operating Characteristic (ROC)	It plots the TPF versus the FPF	-
Area under the curve (AUC)	The area under the ROC (AUC=1 in an optimal system)	$AUC = \int_0^1 TPF(FPF)\, dFPF$
Mathew's correlation coeffcient (MCC)	Used in machine learning as a measure of the quality of binary (two-class) classifications	$\frac{TP \times TN - FP \times FN}{\sqrt{(TP + FP)(TP + FN)(TN + FP)(TN + FN)}}$
F-score	Measure of a test's accuracy	$2 \times \frac{PPV \times Se}{PPV + Se}$
Euclidean distance (D)	Measure the distance between two points in a 2D space. If P(p1,p2) and Q(q1,q2)	$d(P,Q) = \sqrt{(q1 - p1)^2 + (q2 - p2)^2}$

Table 3 – List of the reviewed methods regarding retinal image anatomical features and their outcome results

	Authors	Methods	Databases	Performances
Optic Nerve	Issac *et al.* [43]	Adaptive image thresholding to identify OD and OC boundaries	Local Dataset	Se 100%, Sp 90.0%, Acc 94.4%.
	Dashtbozorg *et al.* [24]	Sliding Band Filter.	MESSIDOR; INSPIRE-AVR	Acc 99.9%; Acc 99.6%.
	Mookiah *et al.* [49]	Attanassov intuitionistic fuzzy histon segmentation.	Local Dataset	Acc 93.4%, F-score 0.92.
	Cheng *et al.* [52]	Superpixel Classification.	MESSIDOR	AUC 0.800.
	Basit and Fraz [53]	Morphological Operations, Smoothing filters and Watershed Transform.	SHIFA (local database); DRIVE; CHASE_DB1; DIARETDB1	AVG Se 99.2%; AVG Sp 76.2%; AVG Acc 98.9%.
	Reza *et al.* [54]	Curve Operator for automatic OD detection.	STARE; DIARETDB1	Acc 87.7%; Acc 94.4%.
Blood Vessels	Odstrcilik *et al.* [19]	Illumination correction, contrast equalizatrion, 2D Mached filtering, thresholding.	HRF; DRIVE; STARE	Se 78.6%, Sp 97.5%, Acc 95.4%, AUC 0.974; Se 70.6%, Sp 96.9%, Acc 93.4%, AUC 0.952; Se 78.5%, Sp 95.1%, Acc 93.4%, AUC 0.957.
	Akram and Khan [74]	2D Gabor wavelet, multilayer and adaptive thresholding.	DRIVE; STARE	Acc 94.7%; Acc 95.0%.
	Bala and Vijayachitra [75]	Mached filtering, local entropy thresholding, Grey lavel co-occurrence matrix for features extraction and Extreme learning machnine for classification.	DIARETDB0; DRIVE	Se 96.7%, Sp 100%, Acc 97.5%; Se 100%, Sp 94.1%, Acc 95.0%.
	Liskowski and Krawiec [77]	Convolutional Neural Network.	DRIVE; STARE	Acc 95.0%, AUC 0.97; Acc 95.7%, AUC 0.979.
	Azzopardi *et al.* [78]	Difference-of-Gaussians filtering (*B*-COSFIRE).	DRIVE; STARE; CHASE_DB1	Se 76.6%, Sp 97.0%, Acc 94.3%, AUC 0.961; Se 77.2%, Sp 97.0%, Acc 95.0%, AUC 0.956; Se 75.9%, Sp 95.9%, Acc 93.9%, AUC 0.949.
	Wang *et al.* [81]	Multiwavelet kernels vessel enhancement, hierarchical optimal decomposition, adaptive thresholding.	DRIVE; STARE	Acc 94.6%; Acc 95.2%.
Macula & Fovea	Chin *et al.* [86]	OD location and vasculature map via geometrical approximation and VAMPIRE, location of the ROI via anatomical priors and fovea location with highest likelihood after 2D Gaussian mask filtering.	Local Dataset; MESSIDOR	Fovea detection rate (FDR) within 25%DD 77.3%, FDR 50%DD 92.4% (with good quality images); FDR 25%DD 56.2%, FDR 50%DD 79.8% (with no risk of macula aedema images).
	Zheng *et al.* [87]	OD location via thresholding, morphological bottom-hat transform for blood vessel elimination, OD boundary detection and circle fitting, fovea location via anatomical constraints and morphological geodesic transform.	DRIVE; HEI-MED; DIARETDB1	FDR 100%; FDR 98.8%; FDR 93.3%.
	Medhi and Dandapat [82]	OD detection via thresholding, fovea detection via Canny edge detector, Othsu thresholding, Hough transform and anatomical constriants.	DRIVE; DIARETDB1	FDR 100% D 6.88; FDR 95.51%, D 8.90.

Table 4 – List of the reviewed methods regarding retinal image abnormalities and their outcome results

	Authors	Methods	Databases	Performances
Abnormalities	Zhang *et al.* [92]	Removal of known anatomical 'bright' features, classification of any remaining 'bright' areas.	e-optha EX; DIARETDB1v2; MESSIDOR; HEI-MED	AUC 0.950; AUC 0.950; AUC 0.930; AUC 0.940.
	Mookiah *et al.* [34]	Local configuration Pattern analysis and statistical ranking.	STARE, ARIA	Acc 97.6%; Acc 90.7%.
	Mookiah *et al.* [35]	Empirical Mode Decomposition.	STARE, ARIA	Acc 100%; Acc 85.1%.
	Figueirdo *et al.* [95]	Binary Classifiers to identify lesion tpye - Analysis of wavelet bands.	Local Datasets (Retmarker)	**Microaneurysms -** Se 93.0%, Sp 89.0%, **Hemorrhages** - Se 86.0%, Sp 90.0%, **Bright Lesions** - Se 90.0%, Sp 97.0%.
	Seoud *et al.* [96]	Dynamic Shape Features.	MESSIDOR	AUC 0.899 (Lesion Detection), AUC 0.916 (Image classification - referable/non-referable).

Figure 1 – Optic disc and optic cup in fundus image. Reproduced with permission from [46]

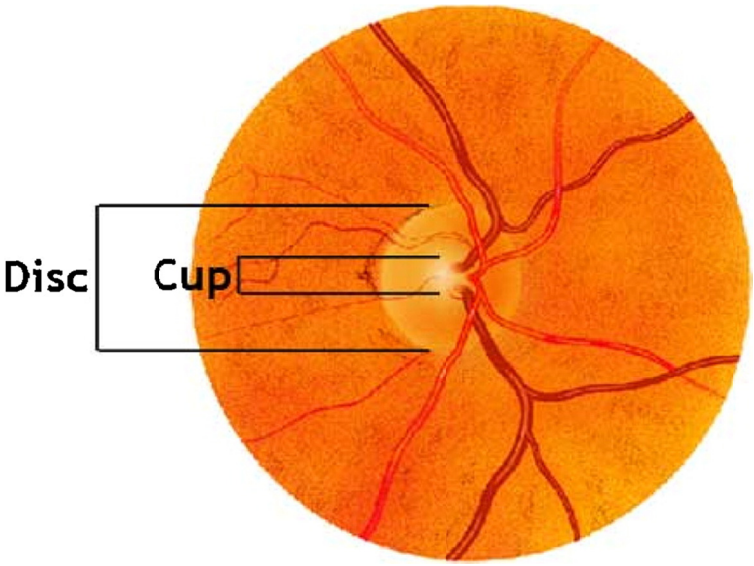

Figure 2 – (a) Example of colored fundus image and (b) binary map of the corresponding manually segmented vessel tree. Reproduced with permission from [76]

Figure 3 – Broad overview of fundus images containing pathology: (a) Normal; (b) Mild NPDR; (c) Moderate NPDR; (d) Severe NPDR; (e) Prolific DR; (f) Macular edema. Reproduced with permission from [37]

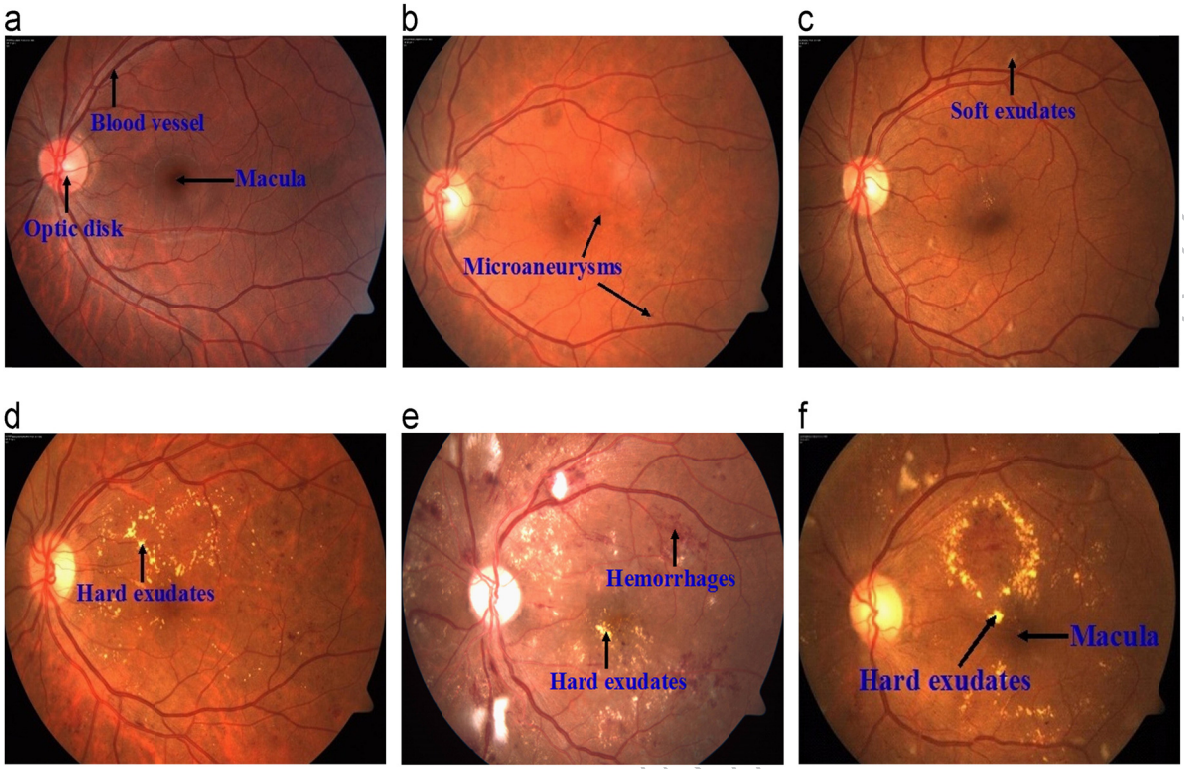

List of Abbreviations

1. DR diabetic retinopathy
2. AMD age-related macular degeneration
3. ONH optic nerve head
4. OD optic disc
5. OC optic cup
6. TP true positive
7. TN true negative
8. FP false positive
9. FN false negative
10. FOV field of view
11. Acc Accuracy
12. Se Sensitivity
13. Sp Specificity
14. SBF sliding band filter
15. ROI region of interest
16. AUC area under the curve
17. B-COSFIRE bar-selective combination of shifted filter responses
18. DD disc diameter
19. NCD number of correct detections
20. FDR Fovea detection rate